Assembly, integration and test of the Layer Oriented Wave Front Sensor for MAD

Matteo Lombini*[a,b], Roberto Ragazzoni[b,d], Carmelo Arcidiacono[g], Andrea Baruffolo[c], Raffaella Bisson[f], Angela Brindisi[b], Julian Coyne[h], Emiliano Diolaiti[a,b], Jacopo Farinato[b], Brice Le Roux[b], Gianluca Lombardi[b,c], Enrico Marchetti[e], Gianluigi Meneghini[f], Elise Vernet[b], Marco Xompero[b]

[a] - Osservatorio Astronomico di Bologna (Italy)
[b] - Osservatorio Astrofisico di Arcetri (Italy)
[c] - Osservatorio Astronomico di Padova (Italy)
[d] - Max-Planck-Institut für Astronomie (Germany),
[e] - European Southern Observatory (Germany)
[f] - NIDEK Tecnologies- Padova (Italy)
[g] - Università di Firenze (Italy)
[h] - Universite de Strasbourg (France)

Abstract

MAD[5] is a Multi-Conjugate Adaptive Optics (MCAO) system conceived to demonstrate the feasibility of MCAO on the sky. The wave front sensor part is divided in two channels: a Shack-Hartmann sensor and a Layer Oriented sensor. We will describe the construction of the latter one. Assembly, integration and test of the instrument are the first steps for ESO acceptance, before integrating the Layer Oriented sensor with the other components of MAD. We will show qualitative and quantitative results of optical and mechanical tests: in particular we will describe the alignment of the references selection unit, constituted by sixteen motorized linear positioners and eight star enlargers, of the beam compressor and of the two re-imaging objectives, each one conjugated to a different altitude. Being the pyramid the core of this kind of wave front sensor, we will focus our attention on its construction difficulties and we will discuss all the optical tests made to choose the best ones to be installed on the wave front sensor. Finally we will present the sensor performance showing the first open loop results.

Keywords: Multi-Conjugate Adaptive Optics systems, Layer Oriented MCAO, Wave Front Sensors.

* matteo@arcetri.astro.it

Advancements in Adaptive Optics, edited by Domenico Bonaccini Calia, Brent L. Ellerbroek, Roberto Ragazzoni, Proceedings of SPIE Vol. 5490 (SPIE, Bellingham, WA, 2004)
0277-786X/04/$15 · doi: 10.1117/12.551567

Introduction

MAD[5] stands for Multi Conjugate Adaptive Optics Demonstrator and it is an instrument that ESO is building with the scope is to prove the applicability of wide field correction of the atmospheric turbulence using the light of natural guide stars (NGS). The system can switch between two different wave front sensors (WFS) just tilting a flat mirror. The atmospheric disturbance will be corrected by two deformable mirrors (DM). One sensor, based on the Star Oriented (SO) approach, has three Shack-Hartmann WFSs that can be moved in the field for reference selection. The Layer Oriented (LO) WFS for MAD is a pyramid based[10] sensor which can sense up to 8 NGS in a circular FoV of 2'. The light coming from the reference stars is collected by the so-called star enlargers[1] and then halved by a beam splitter in two beams in order to feed, using two objectives, the light to the two detectors conjugated at the same altitudes where the DMs are located. This system has therefore a feature typical of the LO approach, where the complexity grows with the number of DMs rather than the number of references, like it is in the SO approach. The light coming from the different references is optically co-added on the detectors. In this way it permits the use also of faint sources for wave front sensing since all of them contribute to increase the SNR on the detector. The result is an increased probability to find suitable references and a decent sky coverage even using only NGS. The scientific camera (CAMCAO) is a 2k by 2k Nyquist sampled camera operating in the K-band having 1'x 1' of FoV.

1 LO-WFS for MAD

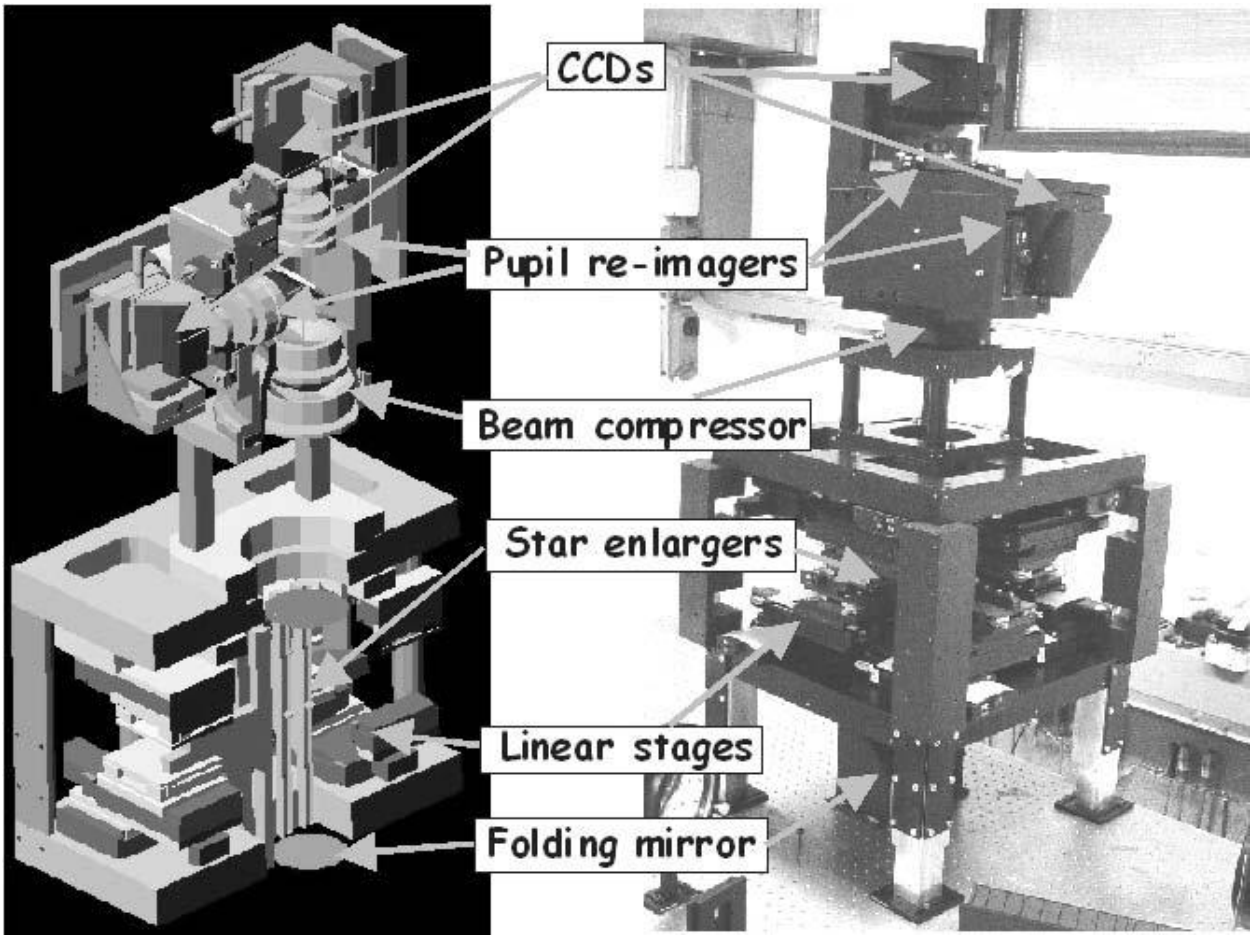

Figure1: On the left a CAD 3-D drawings of the LOWFS for MAD. On the right a picture of the sensor in the Arcetri Lab.

The F/20 beam coming from the telescope is folded into the sensor by a mirror. The images of the GSs are splitted in four parts by the pyramids. The beam compressor reduce the beam dimensions, a beam splitter halves the light between the two objectives which re-image the four pupils onto the two CCDs. One CCD is conjugated at the ground and the other at 8.5 km above the telescope aperture, following the choices of ESO concerning the conjugation altitude of the DMs.
The pyramids are placed at the focal plane of MAD. The small size of the chosen sensor for the LOWFS made us increase the F/20 beam coming from the telescope into an F/300 in order to fit the pupil dimension into the CCD[11]. This increase of the f-number was reached introducing before each pyramid a couple of lenses that magnify the reference star dimension maintaining the telecentricity. From this feature the name Star Enlarger.

2. Error budget

We made a complete error budget of the LOWFS in order to take into account every possible source of error that will reduce the performance of the instrument in terms of wave front quality and, consequently, in term of delivered Strehl. The requirement is that the LOWFS shall deliver a SR > 90% in the K-band at the entrance of the scientific camera corresponding to a maximum WFE of 115 nm. The table 1 summarizes the maximum sub-component contributions to the error sources. The contribution of the motorized stages tilt is taken into account in the star enlarger case. We assumed the environment error source the whole residual of the given maximum wave front error because it is an unpredictable error source.

Item	Maximum WFE contribution
Stars Enlargers	40 nm
Pyramids	50 nm
Pupil re-imaging	40 nm
Chromatism	50 nm
Environment	70 nm
TOTAL	**115 nm**

Table 1: maximum WFE contributions for the various LOWFS sub-systems. The total WFE corresponds a sensor performance that gives a SR > 0.9 in K band.

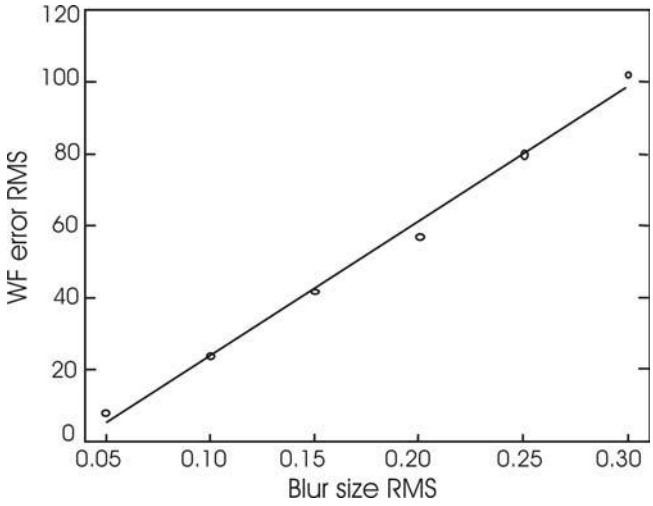

Figure 2: The picture shows the relation between the RMS of the wave front error (the blur size RMS) and the error in the computed correction. The values are expressed in nm.

One can go from the WFE introduced by the sensor to the Strehl Ratio performance using the approximated formula:

$$\sigma = \frac{2\pi}{\lambda} \cdot WFE$$

$$SR = e^{-\sigma^2}$$

where σ is the phase variance in radians and λ is the working wavelength in nanometers.

3 Subsystem tests

The AIT of the LOWFS for MAD started with the tests of its sub-systems and components. For all the alignments and tests we used a collimated laser beam[1]. A telescope simulated has been built in order to perform the open loop tests of the sensor. Lenses and mirrors used in the set ups are commercial ones and for measurement error calculations we had to take care of these optical components contributions, which are anyway static aberrations. Having to test a tenth of pyramid, 18 linear stages, 20 lenses, etc., we made all tests easily repeatable. The collimation was done placing after the laser emitter a spatial filter and a collimating lens at its focal length from the spatial filter, verifying frequently the wave front planarity. An iris after the lens could make the beam dimension vary. Since the LOWFS will use the optical co-add of the light the performance similarity of the star enlargers and of the pyramids is very important, to minimize the aberrations and the pupil displacement alt the level of the detectors. In the following subsections are explained the LOWFS sub-system tests and integrations.

3.1 Linear stages

For 8 SE we need 16 motorized linear stages. Two more stages are used for the CCDs focus positioning. Each star enlarger is moved in the field of view by a couple of motorized linear stages to which they are attached with an arm. The pitch and the roll of the stages plates can induce a tilt during the SE positioning, introducing a misalignment of the references beams and causing a bad superimposition of the pupils on the CCD respect to the nominal position. So we tested all the stages in pitch and in roll to verify their values (fig. 3 left). Several stages were out of spec (pitch and roll below 10'') and have been sent back to the producer for being re-machined and tested again when received back. The two worst stages were chosen to move the CCDs because the requirement in term of pitch and roll is much more relaxed. The linear stages were coupled and disposed in the way to have their movement orthogonal within the tolerances in yaw of a single linear stage. To do that we used a dihedron whose perpendicularity was within five arc seconds.

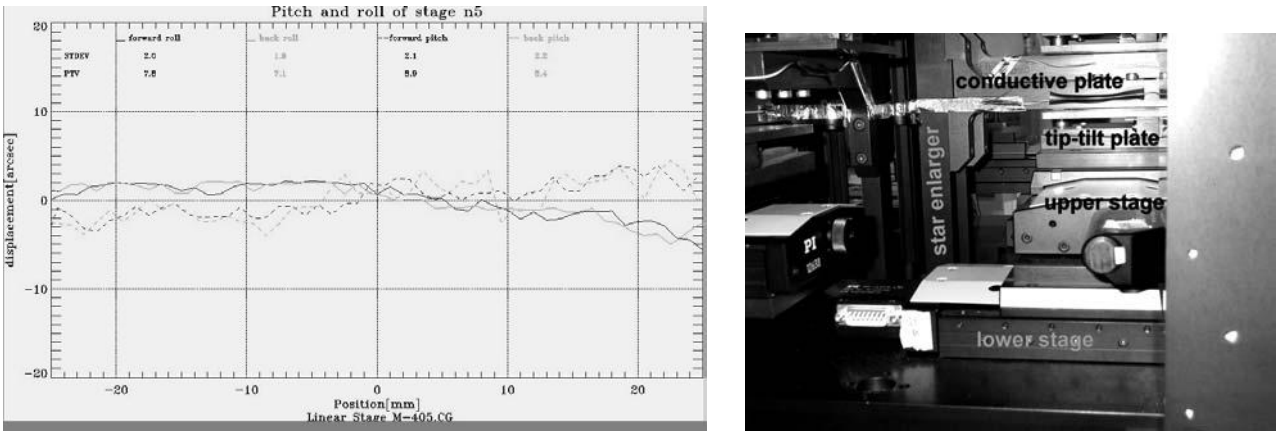

Figure 3: In the left there is plotted a measurement of the pitch and the roll of a motorized linear stage. In the right there is a picture of two linear stages mounted orthogonally into the LOWFS structure.

3.2 Star enlargers

The star enlargers are formed by two lenses inserted into barrels supported by a mechanical structure (fig. 4). The lens 1 has a diameter ϕ = 6 mm and a focal length f_1 = 10 mm, the lens 2 has a diameter ϕ = 12.7 mm and a focal length f_2 =150 mm. The lens 1 is placed at the distance f_1 from the telescope focus. The lens 2 is at the distance $f_1 + f_2$ from the lens 1 so that the exit beam is telecentric. At the end of the SE, at the focus of the lens 2, is placed the pyramid. All the lenses of the star enlargers have been tested to respect to the focal length, transmission and curvature center position. The choice of the couples of lenses was done with the claim to have the most similar magnifications for all the star enlargers. After having measured the focal lengths of the lenses we chose the couples that gave the closest magnification mean value to the nominal one. The lenses could not be adjusted in tilt and only lens 1 could be adjusted in decentering, so the SEs had been aligned optically, anyway trying to make the optical axis as close as possible to the mechanical one. The global tilt of these devices might introduce a displacement of the pupil images. The positioning of lens 2 was done verifying the collimation of the outcoming beam. We recall that a different magnification gives a different pupil size. The positioning of the pyramid in the lens 2 focus is not so critical due to the big focal depth (about 10 mm). The fine positioning of the whole SE is done when testing the static aberrations and it will discussed in section 4.1.

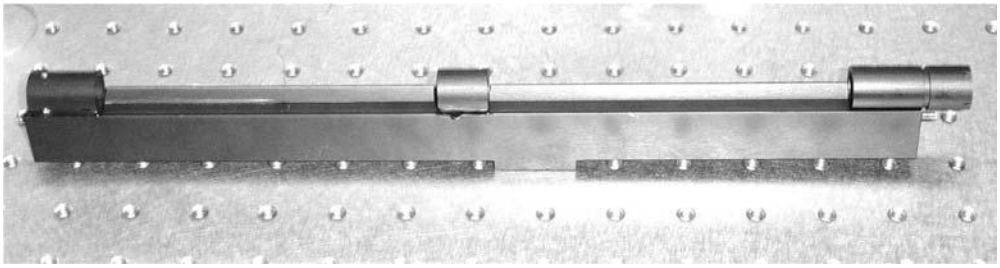

Figure 4: A picture of a star enlarger. The Lens 1 (on the left) and the pyramid (on the right) barrels are blocked by a screw while the lens 2 barrel (in the center) is glued to the star enlarger.

3.3 Pyramids

The pyramids are the core of the layer oriented wave front sensing. A good working of the optical and the mechanical parameters is fundamental for a gainful wave front sensing. The similarity among the vertex angles gives a similarity in the beam divergence i.e. a proper pupil overlapping. We tested the most critical parameters as listed in table 2. The vertex angles were measured using the diffraction image on the CCD when the pyramid is crossed by a collimated beam which is separated into four beams whose direction depends on the relative inclination of the four faces. The turned edges measurements gave us some problems in data interpretation (fig. 5 right). An independent measure preformed in Heidelberg using an electronic microscope gave results very close to ours. We are very satisfied of the pyramids because the differences among the vertex angles of the eight pyramids chosen to be mounted in the WFS will contribute to a pupil blur less than 1/20 of pupil sub-aperture size.

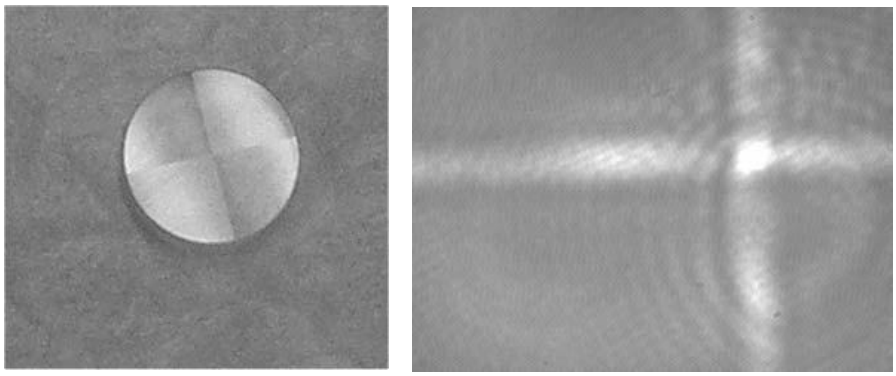

Figure 5: On the left a picture of a pyramid. On the right a magnified image of the turned edges taken in Arcetri's laboratory

	Pyr	Vertex angle		Transmission	Turned edges	Surface flatness	Pin centering
Specs	nº	1.176º ± 0.005 º		> 96 %	< 20 μm	< 2 λ @ λ=633 nm	< 0.1 mm
Test Data	2	1.178 ± 0,003	1.175 ± 0,001	√	15 ± 0,5	√	√
	3	1.176 ± 0,003	1.176 ± 0,004	√	24 ± 0,5	√	√
	4	1.170 ± 0,002	1.174 ± 0,001	√	23 ± 0,5	√	√
	5	1.170 ± 0,003	1.171 ± 0,001	√	22 ± 0,5	√	√
	6	1.169 ±0,003	1.171 ± 0,001	√	21 ± 0,5	√	√
	8	1.172 ± 0,002	1.171 ± 0,001	√		√	√
	9	1.173 ± 0,002	1.175 ± 0,003	√	21 ± 0,5	√	√
	10	1.166 ± 0,003	1.171 ± 0,002	√	23 ± 0,5	√	√
	11	1.174 ± 0,003	1.173 ± 0,003	√	21 ± 0,5	√	√
	14	1.174 ± 0,003	1.173 ± 0,002	√	22 ± 0,5	√	√

Table 2: Data from pyramid measurements. ESO received 13 pyramids from the company and sent us the best ten ones. The pyramid 8 presents a defect in the vertex and it is been discarded

3.4 Objectives alignments

The beam compressor and the two pupil re-imagers are composed respectively of four and three lenses closed in cylindrical boxes. The internal alignments were successfully done by the constructor factory. Before the objective alignments we defined an optical axis centering the incoming laser beam respect to the mechanical structure of the sensor by tilting the folding mirror at the bottom of the structure. The alignment of the beam compressor and of the two pupil re-imagers was done using the Newton's rings that are formed by the back reflected spots of the lenses. The tolerances of the tilt were of 0.01º for the beam compressor and of 0.15º for the pupil re-imagers. The decentering was not critical. Due to its dimensions, the alignment of the beam compressor was quite difficult so we decided, once its position was very close to the theoretical one, to tilt the folding mirror for the final tuning of the alignment In fact the pupil re-imagers had a big tilt adjusting system so they could be aligned also with respect to this new optical axis. The positioning of the beam splitter was done by placing a flat mirror at the CCD position and checking the back reflected spot.

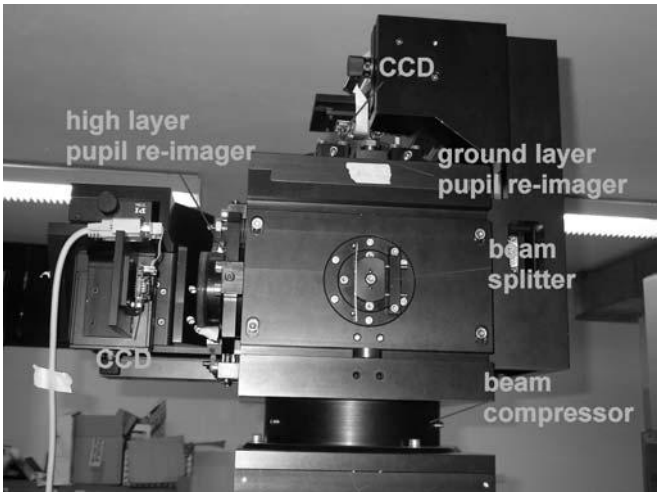

Figure 6: Superior sub-system of the LOWFS.

4 Telescope simulator

The telescope simulator scope is to check the WFS performance. It simulates the F/20 telecentric beam of the VLT, allowing us to test in open loop the LOWFS using white light coming from a set of fibers and a set of perturbing screen to simulate the atmospheric turbulent layers. In figure 7 there is a picture of the telescope simulator set up. The lenses and the diaphragm have been aligned with the laser checking the back reflected spots. The position of the first lens was defined by its distance from the first lenses of the SE. The positioning of the diaphragm and of the re-imaging lens was

made by auto collimation: inserting a target at the pupil position and introducing a flat mirror after the lens we observed the back reflected spot on focus on the pupil plane when the lens was at its focal length *f* from the pupil.

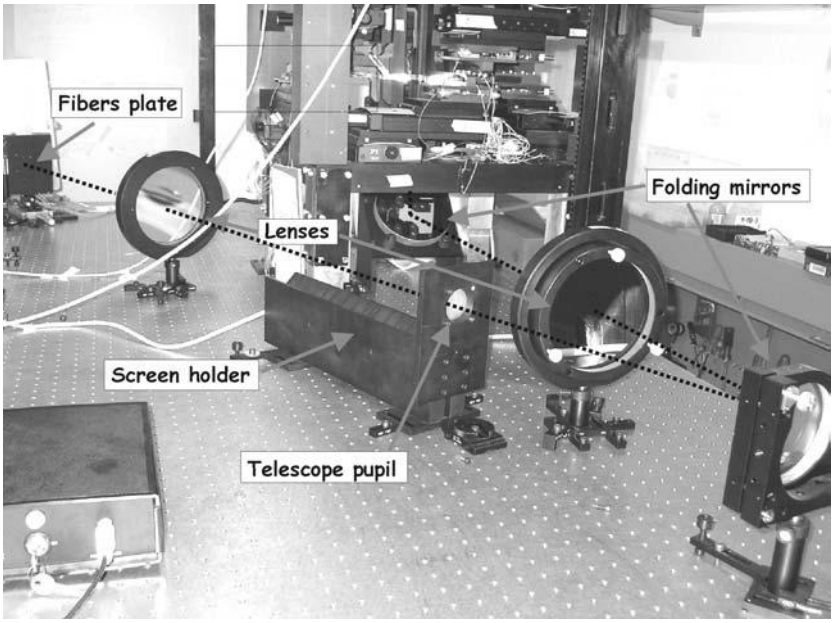

Figure 7: A picture of the telescope simulator.

4.1 Star enlargers alignment

The star enlargers were aligned respect to the laser beam moving them in the center of the field and adjusting the tip-tilt until the spot on the CCD overlapped the spot without the star enlarger. At this point at every SE was attached a conductive plate as it can be seen in fig. 8. In fact during the positioning of them for the reference centering collisions among the SE are possible in case of failure of the control software that, in that case, must be able to stop the motorized linear stages to prevent a destructive crush. The thickness of the conductive plate is 0.8 mm, increasing of few tens of arc seconds the minimum distance among the usable reference stars.

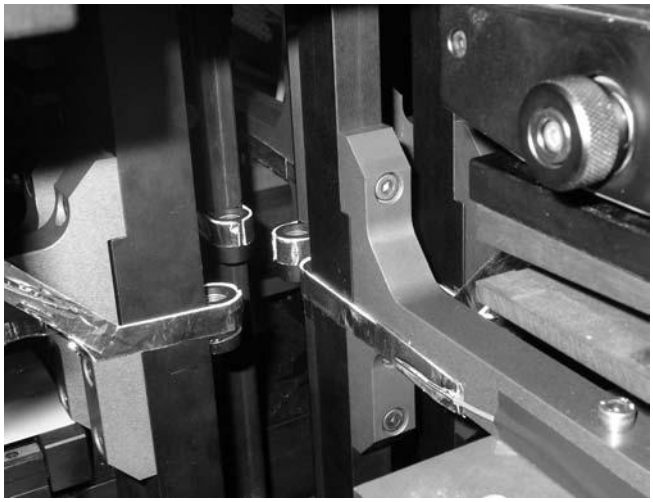

Figure 8: Picture of a reference search units. Above the star enlarger can be seen the conductive plate for the collision control. At the top of the lens 2 there is a gap in the plate in order to make the computer distinguish the side where the contact can happen.

4.2 Wave front calibration

To check the optical quality of the pyramid pupil we had to quantify the static aberrations. The measured wave front was fit with a suitable high number of Zernike polynomials and the Peak-to Valley (PV) of the defocus term was calibrated shifting the fibers of a known quantity and comparing the obtained Peak-to Valley (PV) respect to the expected value given by the formula:

$$PV = \frac{d^2 \delta f}{4 f_0^2}$$

where d = 40 mm is the diaphragm diameter and f_0 = 800 mm is the focal length of the first collimating lens. From the comparison between the expected and the measured value we retrieved the proportionality constant linking the arbitrary units of the computed wave front to the physical units. In figure 9a from left to right there are 4 images of the pupil of the same SE moving of known quantities the fibre plate. The tip-tilt was removed and it can be seen the increasing of the defocus term. In figure 9b also the defocus was removed and only higher order aberrations remain. The residual wave front RMS is of the order of 100 nm. In this value one mast take into account also the telescope simulator contribution that was not calculated in the top level requirement (see table 1) and ray tracing calculations show that the computed error is in line with the measured one. A first test of the optical quality of the system was done by placing a mask on the pupil plane. In this mask there are several holes with a diameter of 0.8 mm. The telescope pupil diameter of 40 mm and the pupils size on the CCD measures 52 pixels. If the images of these circles on the CCD have a FWHM of 1 pixel the overall optical quality does not blur the wave front more than our specifications. Such it is.

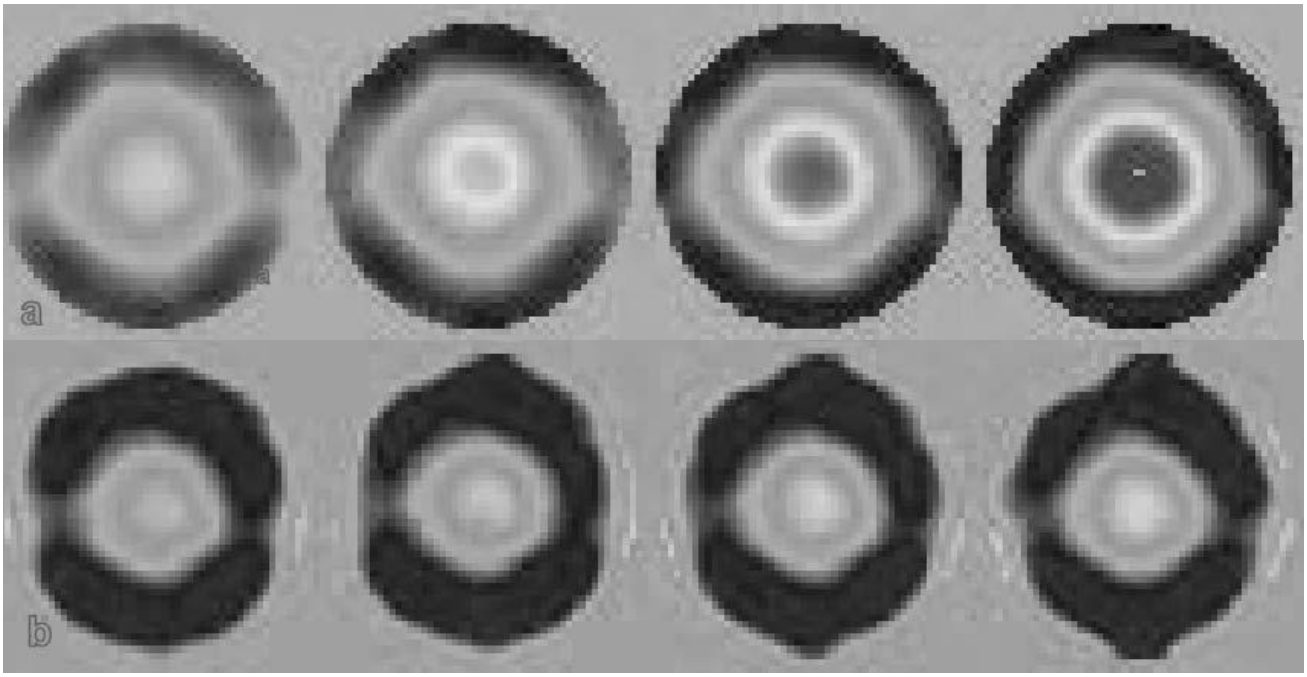

Figure 9: a) Pupil image of the same star enlarger moving the fibers plate in four positions. The tip-tilt was removed and it can be seen the increase of the defocus aberration. In this way we could quantify this aberration. b) The same images with the defocus removed.

4.2 Final tests

To conclude the tests on the sensor performance we have to check the optical quality of the overlapped pupils. To do this we need the motion controllers that will arrive soon from ESO. We will perform correlation tests placing screens conjugated to different heights using several star asterisms. In fact a property of the layer system is to be more sensitive

to the nearest perturbing layers from the focusing altitude and we have to quantify how much the screens out of focus influence the wave front measures.

5. Conclusions

The LOWFS assembly, integration and test (AIT) is at the final step. At the end of September there should be the Preliminary Acceptance Europe from ESO. After it the sensor will be sent to Garching to be integrated into MAD and perform close loop runs with deformable mirrors and a dynamic aberration simulator (MAPS)[13].
When one passes from drawing to metal a myriad of problems rises. We had to deal with construction imperfections, to invent the sets up for the tests, to calculate the errors of our measurements. Anyway we have acquired an experience that will be useful for the next instruments. For example the design of NIRVANA, the LOWFS for the LBT MCAO system, has been done taking care of this experience: many little tricks to simplify the integration are necessary for a sensor that will have twelve star enlargers and that will be a permanent instrument and not only a demonstrator like MAD. Anyway we hope that MAD performances will convince everyone that the MCAO is a winning bet and that its use will be not limited to some short planned demonstration runs but we are confident that even this demonstrator could be used for serious and so far inaccessible science targets for ground based telescopes.

Acknowledgements

Thanks to Joana Costa end Stefan Hippler for their independent measurement of the pyramid turned edges. Thanks to Armando Riccardi for his helpfulness and to Paolo Stefanini for satisfying all our requests of building little tools for laboratory working

References

1. Matteo Lombini, “Ottica adattiva a grande campo per il VLT”,Osservatorio Astronomico di Bologna, 2003
2. Vernet E., Ragazzoni R., Diolaiti E., Farinato J., Bariffolo a., Arcidiacono C., Crimi G., Ghigo M., Tomelleri R., Rossettini F., ”Layer Oriented WFS Prototype Test Report”, Doc. No.: OWL-TRE-INA-600000-0054, Issue:2.0
3. Farinato J.,Viard E., Ragazzoni R., Baruffolo A., Diolaiti E., Arcidiacono C., “Layer Oriented WSF Assembly Integration and test plan”, Doc. No.: OWL-PLA-INA – 60000-0065, Issue:1.0
4. Diolaiti E., Farinato J., Ragazzono R., Viard E., Baruffolo A., Arcidiacono C., Carbillet M., “Layer Oriented WFS Final Design”, Doc. No.:OWL-TRE-INA-60000-0055, Issue:1.1
5. Marchetti E., Hubin N., Fedrigo E., Brynnel J., Delabre B., Donaldson R., Franza F., Conan R., Le Louarn M., Cavadore C., Balestra A., Baade D., Lison J.-L., Gilmozzi R., Monnet G., Ragazzoni R., Arcidiacono C., Baruffolo A., Diolaiti E., Farinato J., Viard E., Butler D., Hippler S., Amorim A., "MAD the ESO multi-conjugate adaptive optics demonstrator", SPIE Proc. **4839**, pp. 317-328, 2003
6. Ragazzoni R., Farinato J., Diolaiti E., Viard E., Baruffolo A., Arcidiacono C., “Multi Coniugate Adaptive Optics Demonstrator Real Time Computer”, Doc. No.: OWL-SPE-INA 60000- 0061, Issue:1.0
7. Farinato J., Ragazzoni R., Diolaiti E., Vernet-Viard E., Baruffolo A., Arcidiacono C., Ghedina A., Cecconi M., Rossettini P., Tomelleri R., Crimi G., Ghigo M., "Layer oriented adaptive optics: from drawings to metal", SPIE Proc. **4839**, pp. 588-599, 2003.
8. Beckers J. M., “Increasing the size of the isoplanatic patch size with multiconjugate adaptive optics”, in *ESO conference on Very Large Telescopes and their instrumentation*, M.-H. Hulrich, ed., pp. 693, 1988.
9. Ragazzoni R., Diolaiti E., Farinato J., Fedrigo E., Marchetti E., Tordi M., Kirkman D., "Multiple field of view layer-oriented adaptive optics. Nearly whole sky coverage on 8 m class telescopes and beyond", A&A **396**, 731-744, 2002.
10. Ragazzoni R., “Pupil plane wave front sensing with an oscillating prism”, *J. of Mod. Opt.* **43**, pp. 289-293, 1996.
11. Ragazzoni R., Diolaiti E., Vernet E., Farinato J., Marchetti E., "Arbitrarily small pupils in layer-oriented multi-conjugate adaptive optics", PASP, accepted for publication.
12. Ragazzoni R., Farinato J., “Sensitivity of a pyramidic wavefront sensor in closed loop adaptive optics”, *A&A* 350, pp. L23-L26, 1999
13. Butler D., Marchetti E., Bahr J., Xu W., Hippler S:, Kasper E:, Conan R.,” Phase screens for astronomical multi-conjugate adaptive optics: application to MAPS”, SPIE proc. 4839 pag. 623B, 2003